Experimental investigation of high-spin states in ^{90}Zr

P. Dey,[1,*] D. Negi,[1,†] R. Palit,[1,‡] P. C. Srivastava,[2] Md. S. R. Laskar,[1] B. Das,[1] F. S. Babra,[1] S. Bhattacharya,[3] Biswajit Das,[1] K. Rojeeta Devi,[4] R. Gala,[1] U. Garg,[5] S. S. Ghugre,[6] E. Ideguchi,[7] S. Kumar,[4] A. Kundu,[1] G. Mukherjee,[8,9] S. Muralithar,[10] S. Nag,[11] S. Nandi,[8,9] Neelam,[4] M. Kumar Raja,[12] R. Raut,[6] R. Santra,[1] A. Sharma,[13] S. Sihotra,[14] A. K. Singh,[15] R. P. Singh,[10] and T. Trivedi[3]

[1] *Department of Nuclear and Atomic Physics, Tata Institute of Fundamental Research, Mumbai 400005, India*
[2] *Department of Physics, Indian Institute of Technology Roorkee, Roorkee 247667, India*
[3] *Department of Pure & Applied Physics, Guru Ghasidas Vishwavidyalaya, Bilaspur 495009, India*
[4] *Department of Physics & Astrophysics, University of Delhi, Delhi 110007, India*
[5] *Physics Department, University of Notre Dame, Notre Dame, Indiana 46556, USA*
[6] *UGC-DAE CSR Kolkata Centre, Kolkata 700098, India*
[7] *Research Center for Nuclear Physics, Osaka University, Ibaraki, Osaka 567-0047, Japan*
[8] *Variable Energy Cyclotron Centre, 1/AF Bidhan Nagar, Kolkata 700064, India*
[9] *Homi Bhabha National Institute, Anushaktinagar, Mumbai 400094, India*
[10] *Inter University Accelerator Centre, Aruna Asaf Ali Marg, New Delhi 110067, India*
[11] *Department of Physics, Indian Institute of Technology (Banaras Hindu University), Varanasi 221005, India*
[12] *Department of Physics, GITAM Institute of Science, GITAM University, Visakhapatnam 530045, India*
[13] *Department of Physics, Himachal Pradesh University, Summer Hill, Shimla 171005, India*
[14] *Department of Physics, Panjab University, Chandigarh 160014, India*
[15] *Department of Physics, Indian Institute of Technology Kharagpur, Kharagpur 721302, India*

(Received 13 December 2021; accepted 23 March 2022; published 11 April 2022)

High-spin states of ^{90}Zr have been investigated using the heavy-ion fusion-evaporation reaction ^{82}Se(^{13}C, $5n$) at a beam energy of 60 MeV. Excited levels of ^{90}Zr have been observed up to an excitation energy of $\approx$13 MeV and a spin of $\approx 20\hbar$ with the addition of thirty-two new γ-ray transitions to the proposed level scheme. Structures of both the positive- and negative-parity states up to the highest observed spin have been interpreted with shell-model calculations using the GWBXG interaction and a ^{68}Ni core. Calculations suggest the role of neutron excitations across the $N = 50$ shell gap for states with greater than 7 MeV excitation energy. High-spin states in these bands are interpreted to be generated by the recoupling of stretched proton and neutron configurations.

DOI: 10.1103/PhysRevC.105.044307

I. INTRODUCTION

Nuclei in the vicinity of shell closures are of particular interest in nuclear structure studies because they provide a platform for scrutinizing the validity and details of shell-model theories. It is now computationally feasible to extend shell-model calculations to higher excitations that incur a larger model space and an increased number of valence nucleons, to be used for the purpose. High-spin states in the $A \approx 90$ mass region, with $Z \approx 40$ and $N \approx 50$, have been subjects of investigation in many studies, both experimentally and theoretically [1–31]. These states have multiquasiparticle configurations, with the $g_{9/2}$ orbital playing a significant role towards the generation of high-spin states. The contribution of proton $g_{9/2}$ orbital comes into the picture either due to the (proton) particle occupancy of the orbital, which is for nuclei with $Z > 40$, or due to excitations of protons from the fp orbitals into the $g_{9/2}$ orbital across the $Z = 40$ subshell gap. These excitations dominate the lower-energy part of the level scheme in these nuclei. Similarly, the role of neutron $g_{9/2}$ orbital towards the high-spin generation is seen to be either due to the already-present holes in it, which is the case for nuclei with $N < 50$, or to excitations across the $N = 50$ shell gap into the gd orbitals. Due to the larger energy of this gap, the contributions from these excitations underlying the high-spin states in $N = 50$ nuclei are observed at higher excitation energies. Such excitations of one or more neutrons from the $1g_{9/2}$ orbital into the $2d_{5/2}$ and $1g_{7/2}$ have been observed in the ^{86}Kr ($Z = 36$) [2], ^{87}Rb ($Z = 37$) [4], ^{88}Sr ($Z = 38$) [6], ^{89}Y ($Z = 39$) [11,12], ^{91}Nb ($Z = 41$) [21], ^{92}Mo ($Z = 42$) [23], ^{93}Tc ($Z = 43$) [27], ^{94}Ru ($Z = 44$) [29], and ^{95}Rh ($Z = 45$) [31] isotones, but it has yet to be confirmed in ^{90}Zr ($Z = 40$) [15]. The shell-model calculations have been used to describe observed excited states based on either proton excitation across $Z = 40$ or neutron excitation across $N = 50$. It will be intriguing to invoke the two excitations simultaneously for ^{90}Zr, which is the focus of the present study.

---

[*] piku.dey@tifr.res.in
[†] dinphysics@gmail.com
[‡] palit@tifr.res.in

Shell-model calculations with the $\pi[1f_{5/2}, 2p, 1g_{9/2}]$, $\nu[2p_{1/2}, 1g_{9/2}]$ model space have been able to reproduce the experimental data reasonably well in ^{83}Br [32], ^{85}Rb [32], and ^{87,88}Y [8,10] up to a certain excitation energy ($\approx$5 MeV). The model space clearly seems to be inadequate for the description of high-spin states at higher excitation energies, where the role of $\nu[1g_{9/2}, 2d_{5/2}, 1g_{7/2}]$ orbitals due to excitation across the $N = 50$ shell gap increases. This is observed in the study of high-spin states of many nuclei, e.g., ^{88}Sr [6], ^{88}Y [10], and ^{90,91,92}Zr [15,18]. In the present study, shell-model calculations have been performed involving these neutron orbitals to probe the role of these orbitals.

High-spin structures in this mass region have been observed to form $\Delta I = 1$ sequences of either parities with $M1$ transitions [6,8,15–17,33,34]. In ^{87}Y and ^{88}Sr, strong $B(M1)$ values have also been reported [6,8]. The semiclassical model of the shears mechanism has been used to describe a decrease in $B(M1)$ strengths reported in ^{87}Zr [33]. Although such $\Delta I = 1$, $M1$ sequences have been observed in ^{90}Zr by Warburton *et al.* [15], detailed information on the structure of these sequences could not be obtained owing to the inconclusive nature of their parity assignments. Note that the parity assignments of certain states, following the polarization measurements of different γ-ray transitions, are in disagreement. Recently, these sequences have been interpreted as examples of magnetic rotation [35], with the configuration assignments based on the parity assignments of Ref. [15]. The current work reports a detailed spectroscopic investigation of the ^{90}Zr nucleus. It has been directed at identifying new structural features in the high-excitation regime as well as addressing the existing uncertainties in the assignments of properties for previously known transitions. The observed level scheme of the nucleus, up to the highest excitations, has been interpreted within the framework of shell-model calculations with large basis space.

II. EXPERIMENTAL DETAILS AND DATA ANALYSIS

Excited states of ^{90}Zr were populated using heavy-ion fusion-evaporation reactions ^{82}Se(^{13}C, $5n$)^{90}Zr with a 60 MeV ^{13}C beam provided by the TIFR-BARC Pelletron Linac Facility (PLF) at TIFR, Mumbai, India. The target used was a 1-mg/cm^2-thick foil of ^{82}Se with a backing of ^{197}Au foil of thickness 4.3 mg/cm^2. The recoil velocity of the compound nucleus was $\approx 0.014c$. The γ rays emitted in the reactions were detected by the Indian National Gamma Array (INGA) at TIFR, which is a Compton-suppressed clover HPGe detector array with a provision of placing 24 detectors at various angles with respect to the beam direction [36]. During the experiment, a total of eleven clover detectors were placed at different angles, with two at 115°, and three each at 90°, 140°, and 157°. The target-to-detector distance was 25 cm.

The electronic signal generated from the interaction of γ rays with the detector were collected and processed with a digital data-acquisition (DDAQ) system. The DDAQ system was housed in a compact PCI-PXI crate and consisted of six 12-bit 100 MHz Pixie-16 modules developed by XIA-LLC [37]. Each module has sixteen channels collecting signals from the individual crystals of clover detectors. A valid fast trigger of width 100 ns was generated for an event in a given channel of the Pixie-16 module in the absence of a veto pulse from the respective BGO Compton-suppression shield within a specific time window. Each Compton-suppressed clover detector generates a fast trigger of width 100 ns which is used for the gamma multiplicity in an event. Once the two- or higher-fold multiplicity is found, the master trigger was opened for 10 μs. This way, the γ rays below the isomeric state could be found along with the prompt γ rays above the isomer. The data-sorting program, MultipARameter time-stamped based COincidence Search (MARCOS) [38], developed at TIFR, was used for sorting two- and higher-fold coincidence events into different E_γ-E_γ matrices and an E_γ-E_γ-E_γ cube, respectively. The RADWARE software package was used for data analysis [39,40].

For the coincidence analysis, E_γ-E_γ matrices and E_γ-E_γ-E_γ cubes with different time windows (100 ns, 500 ns) around the prompt peak have been investigated. Efficiency and energy calibrations of the INGA are carried out using the ^{152}Eu and ^{133}Ba radioactive sources. The level scheme of the ^{90}Zr nucleus was constructed from the coincidence relationships between the γ rays, their intensities, and their multipolarities and electromagnetic character, as determined through standard analysis techniques of γ-ray spectroscopy.

The spins of the levels are assigned through the measurements of the multipolarities of γ-ray transitions, which in turn are obtained from the angular distribution and directional correlation of oriented states (DCO) methods. The experimental angular distribution is given by the expression [41]

$$W(\theta) = A_0[1 + a_2P_2(\cos\theta) + a_4P_4(\cos\theta)], \quad (1)$$

where A_0 is the normalization parameter, $P_n(\cos\,\theta)$ is the Legendre polynomial of order n, and θ is the angle between the detector position and the beam axis. The angular distribution coefficients a_2 and a_4 were obtained from the χ^2-minimization of $W(\theta)$ to the observed yields at different angles.

The DCO method is incorporated by taking the ratios (R_{DCO}) of intensities of coincident events detected at two different angles [42,43]. In the present geometry of the INGA, R_{DCO} is obtained using the expression

$$R_{\mathrm{DCO}} = \frac{I(\gamma_1) \text{ at } 157^\circ \text{ gated by } \gamma_2 \text{ at } 90^\circ}{I(\gamma_1) \text{ at } 90^\circ \text{ gated by } \gamma_2 \text{ at } 157^\circ}, \quad (2)$$

where $I(\gamma_1)$ represents the intensity of γ_1 measured in coincidence with γ_2. The R_{DCO} values of stretched dipole and quadrupole transitions are $\approx$0.5 (1.0) and $\approx$1.0 (2.0), respectively, in a pure quadrupole (dipole) gate. Intermediate values of R_{DCO} between these values indicate the mixed nature of the transitions.

The parity of an excited state is determined from the linear polarization measurement of the γ-ray transition emitted from that level. To identify the character, detectors at the angle 90° are used since, at this angle, the polarization measurements are most sensitive. This arrangement facilitates the use of clover detectors as Compton polarimeters [46]. To extract the polarization asymmetry, the integrated polarization directional correlation of oriented states (IPDCO) method was employed [47]. The electric or magnetic character of the γ rays are determined from the asymmetry of the Compton-scattered events in parallel and perpendicular directions. The polarization asymmetry of a transition, Δ_{asym}, is defined as

$$\Delta_{\text{asym}} = \frac{a(E_\gamma)N_\perp - N_\parallel}{a(E_\gamma)N_\perp + N_\parallel}, \tag{3}$$

where $N_\perp$ ($N_\parallel$) is the intensity of γ-ray transitions scattered perpendicular (parallel) to the reaction plane and $a(E_\gamma)$ is a correction factor arising from any experimental asymmetry. $a(E_\gamma)$ was determined from the ratio of parallel to perpendicular scattered events of unpolarized γ rays from ^{133}Ba and ^{152}Eu radioactive sources. By fitting the experimentally observed $a(E_\gamma)$ values at different energies with a linear expression, $a(E_\gamma) = x + yE_\gamma$, we obtained $x = +1.013(5)$ and $y = -2.1(8) \times 10^{-5}$ keV^{-1}. This result indicates a negligible dependence of $a(E_\gamma)$ on E_γ over the energy range considered for the purpose.

For the determination of Δ_{asym}, two asymmetric matrices were constructed which contain events corresponding to parallel and perpendicular scattered γ rays inside the 90° detectors in coincidence with γ rays detected by any other detector of the array. A positive Δ_{asym} indicates the stretched $E1$, $E2$ or nonstretched $M1$ transition while a negative value implies stretched $M1$, $M2$ or nonstretched $E1$ transition.

III. RESULTS

The proposed level scheme of ^{90}Zr, resulting from the present analysis, is presented in Fig. 1. Properties of the levels and transitions determined from this work are reported in Table I. There is a 131(4) ns 8^+ isomer at 3588 keV excitation energy (see Fig. 1) which affects the measurements of relative intensities of the transitions across this isomeric state. The placement of transitions below this 8^+ level is made on the basis of relative yields determined from the total projection spectrum and are found to be in agreement with earlier results [15]. The relative intensities of gamma transitions above the 8^+ level are determined from the total projection as well as gated spectra and are normalized to that of the 2055-keV transition which feeds the 8^+ isomer. In the previous work on ^{90}Zr, Warburton *et al.* [15] reported levels up to the excitation energy ≈13 MeV and spin, $I = 20\hbar$, with tentative assignments for the levels above the 10^+ level at $E_x = 5643$ keV. In the present work, thirty-two new transitions have been added to the existing level scheme, and spin-parity of the levels have been determined. Two representative spectra, which are a sum of double-gated spectra, have been generated with gates on previously known γ-ray transitions and are shown in Figs. 2 and 3. These gated spectra were generated from the E_γ-E_γ-E_γ cube with a coincidence time window of 500 ns. For the intensities, R_{DCO} and Δ_{asym} measurements, the same coincidence time window was used. The newly observed γ-ray transitions are marked in red in these figures and placed in the level scheme (Fig. 1). The 2319-keV transition shown in inset (b) of Fig. 2 is emitted in the decay of the 5^- isomeric state and it is essentially a constant background on the timescale of the coincidence windows. In the same gated spectrum (as in Fig. 2) generated with the 100 ns time window, the 2319-keV peak is too weak and gets obscured by the background. This rules out the presence of an additional 2319-keV transition in the level scheme.

Angular distribution measurements of some important γ-ray transitions of energies 818-, 1310-, and 2055-keV have been carried out. The results are in agreement with previously reported multipolarity assignments of these transitions [15]. The angular distribution measurements suggest, namely, $L = 1$ for the 818-, 1310-keV transitions and $L = 2$ for the 2055-keV transition. In Fig. 4, the angular distributions of relative yields, $W(\theta)/A_0$, for the 2055-, 1310- and 818-keV gamma transitions are presented. In addition, the positive values of Δ_{asym} suggest their electric character. These transitions have primarily been used as reference transitions for the R_{DCO} of other transitions in the level scheme. The R_{DCO} and Δ_{asym} measurements for the 213- and 269-keV transitions suggest them as stretched $M1$ and $E1$ transitions, respectively. Additionally, a small mixing ratio ($\delta = +0.034^{+0.037}_{-0.042}$) of the 213-keV transition indicates very little $E2$ mixing and thus it can be regarded as a pure dipole transition. These two transitions are also used as reference transitions for the DCO ratio measurements.

A new sequence of levels, referred to as Band III, has been observed. For clarity in discussion, the whole level scheme is divided into four groups, which are labeled Band I, Band II, Band III, and the other states in Fig. 1.

A. Band I

The levels at 7193, 7222, 7436, 8056, and 8955 keV are included in this band. These levels were observed in the earlier work as well [15], but their spin assignments were tentative. In this study, we have determined the spin-parity assignment of these levels. The spin-parity assignment of the 7222 keV level is confirmed as 12^+ following the determination of the 1310- and 269-keV transitions as $E1$. Above the 12^+ state, the transitions of the band are determined as $M1$. This agrees with the previously reported positive-parity assignment up to the 14^+ level at 8056 keV excitation energy. The 899-keV transition is assigned as $M1$ type based on the polarization measurement which was previously reported as of $E1$ character [15]. The final value of $\Delta_{\text{asym}} = -0.041(5)$ for this transition is obtained by taking the weighted average of Δ_{asym} determined individually from the coincidence spectra with gates on the 213-, 269-, 818-, 1167-, 1310- and 2055-keV transitions. It is important to note that the 898-, 899-, and 901-keV transitions from ^{88}Sr [6], ^{90}Y [13], and ^{91}Zr [18], respectively, can be the contaminants for the polarization measurements for the fusion-evaporation reactions used for the study of ^{90}Zr in the present as well as previous measurement [15]. Gating on transitions of ^{90}Zr ensured the elimination of possible contaminants, especially the one coming from ^{91}Zr. In addition, two weak crossover $E2$ transitions of 834-keV ($14^+ \rightarrow 12^+$) and 1520-keV ($15^+ \rightarrow 13^+$) are confirmed and were reported tentatively in previous work [15].

B. Band II

A sequence of levels interconnected by $M1$ transitions has been observed. This sequence has been observed in the

TABLE I. Table for level energy (E_i) and spin-parity of the states, and γ-ray energy (E_γ), intensity (I_γ), R_{DCO}, Δ_{asym} and multipolarity of the transitions obtained from this work. The γ-ray and level energies are given up to the first decimal values in the table. These values are rounded to the nearest whole numbers in the figures and text.

E_γ [a] (keV)	Intensity (I_γ)[b]	Level energy (E_i) (keV)	DCO ratio (R_{DCO}) $L = 1$ gate[c]	$L = 2$ gate[d]	Polarization asym. (Δ_{asym})	Multipolarity	$I_i^\pi \longrightarrow I_f^\pi$
Below 3588 keV level							
132.7		2319.1					$5^- \longrightarrow 2^+$
140.7		3588.4					$8^+ \longrightarrow 6^+$
328.5		3076.6					$4^+ \longrightarrow 3^-$
370.8		3447.9					$6^+ \longrightarrow 4^+$
429.3		2748.1					$3^- \longrightarrow 5^-$
561.1		2748.1					$3^- \longrightarrow 2^+$
757.4		3076.6					$4^+ \longrightarrow 5^-$
890.1		3076.6					$4^+ \longrightarrow 2^+$
1128.8		3447.9					$6^+ \longrightarrow 5^-$
1270.0		3588.4					$8^+ \longrightarrow 5^-$
2186.4		2186.7					$2^+ \longrightarrow 0^+$
2319.1		2319.1					$5^- \longrightarrow 0^+$
Above 3588 keV level							
29.6[e]		7222.2					$12^+ \longrightarrow 11^+$
54.4	1.81(19)	7007.6					$11^- \longrightarrow 11^-$
151.3	2.31(15)	10122.6	0.92(15)[f]			$M1$[g]	$16^- \longrightarrow 15^-$
168.2	20(2)	7192.8	1.06(11)[h]	0.52(9)		$M1$[g]	$11^+ \longrightarrow 10^+$
213.3	150(12)	7435.6	1.08(8)[i]	0.53(4)[j]	−0.049(7)	$M1$	$13^+ \longrightarrow 12^+$
214.4[k]	26(2)	7222.2	1.03(10)[f]			$E1$[g]	$12^+ \longrightarrow 11^-$
232.2	2.82(15)	6952.8	0.88(9)[l]		−0.019(96)	$M1$	$11^- \longrightarrow 10^-$
269.4	52(3)	7222.2	1.12(6)[f]	0.52(3)	+0.104(7)	$E1$	$12^+ \longrightarrow 11^-$
287.0	12.27(94)	7007.6	0.96(8)[h]	0.55(8)	−0.016(38)	$M1$	$11^- \longrightarrow 10^-$
289.2	12.00(52)	10122.6	0.89(6)[f]	0.36(4)	−0.070(42)	$M1$	$16^- \longrightarrow 15^-$
344.8	8.54(43)	6720.0	2.07(17)[h]		+0.096(32)	($E2$)	$10^- \longrightarrow 10^-$
386.4	1.19(8)	10761.7					$17^- \longrightarrow 16^-$
396.4	1.07(5)	5643.2					$10^+ \longrightarrow 9^+$
403.2	5.05(33)	10374.7	0.87(9)[i]	0.41(5)	−0.073(32)	$M1$	$16^- \longrightarrow 15^-$
429.2[m]	3.83(10)	6706.3	0.78(8)[h]		−0.043(65)	($M1+E2$)	$\longrightarrow 11^+$
443.1	≈0.5(1)	6720.0					$10^- \longrightarrow 11^+$
450.8	4.16(44)	12556.9	1.21(12)[h]		−0.017(75)	$M1+E2$	$20^{(-)} \longrightarrow 19^-$
470.3	1.60(8)	9333.5					$15^+ \longrightarrow 14^-$
483.1	2.17(19)	11354.2	0.92(8)[h]	0.61(5)	−0.048(53)	$M1$	$18^- \longrightarrow 17^-$
489.3	<0.5	6766.4					$\longrightarrow 11^+$
496.3	4.78(42)	10871.1	0.82(7)[h]		−0.032(24)	$M1$	$17^- \longrightarrow 16^-$
528.4	4.32(32)	11399.3	0.86(9)[h]		−0.086(60)	$M1$	$18^- \longrightarrow 17^-$
541.1	4.03(24)	10374.7	1.11(9)[h]		−0.026(30)	$M1$	$16^- \longrightarrow 15^-$
583.3	11.41(69)	6374.8	0.83(3)[i]		+0.035(24)	$E1$	$10^- \longrightarrow 9^+$
619.7	111(3)	8055.6	0.79(2)[f]	0.35(1)	−0.049(3)	$M1+E2$	$14^+ \longrightarrow 13^+$
633.2	8.99(41)	6277.1					$11^+ \longrightarrow 10^+$
637.4[n]	22(2)	11399.3	0.78(3)[f]	0.44(2)	−0.042(5)	$M1$	$18^- \longrightarrow 17^-$
638.3[n]	36.51(88)	10761.7	0.78(3)[f]	0.44(2)	−0.042(5)	$M1$	$17^- \longrightarrow 16^-$
671.8	2.01(9)	10005.6	0.72(7)[l]		+0.024(18)	($E1$)	$(16^-) \longrightarrow 15^+$
706.8	17(2)	12106.1	1.08(8)[h]		−0.063(11)	$M1$	$19^- \longrightarrow 18^-$
731.1	11.26(31)	6374.8	2.09(12)[i]	0.89(4)	−0.076(21)	$E1$	$10^- \longrightarrow 10^+$
748.7	4.88(46)	10871.1	0.84(7)[h]		−0.128(24)	$M1$	$17^- \longrightarrow 16^-$
755.9	1.15(6)	10761.7					$17^- \longrightarrow (16^-)$
789.3	6.99(22)	10122.6	0.86(9)[f]		+0.033(30)	$E1$	$16^- \longrightarrow 15^+$
808.2	<0.5	8863.3					$14^- \longrightarrow 14^+$
818.0	52(2)	7192.8	0.87(6)[h]	0.55(4)	+0.045(6)	$E1$	$11^+ \longrightarrow 10^-$
833.7	6.45(51)	8055.6	1.51(12)[l]		+0.045(42)	($E2$)[o]	$14^+ \longrightarrow 12^+$
853.1	5.41(55)	12959.2	1.09(9)[h]		−0.055(18)	$M1$	$20^- \longrightarrow 19^-$
878.1	3.62(11)	9833.4	1.47(20)[h]		−0.102(91)	$E1$	$15^- \longrightarrow 15^+$
899.1	43(2)	8955.1	0.90(2)[i]	0.46(2)	−0.041(5)	$M1$	$15^+ \longrightarrow 14^+$

TABLE I. (*Continued.*)

E_γ [a] (keV)	Intensity (I_γ)[b]	Level energy (E_i) (keV)	DCO ratio (R_{DCO}) $L = 1$ gate[c]	$L = 2$ gate[d]	Polarization asym. (Δ_{asym})	Multipolarity	$I_i^\pi \longrightarrow I_f^\pi$
926.6	2.00(18)	12280.8	1.43(18)[h]			$(M1+E2)$	$19^{(-)} \longrightarrow 18^-$
1014.7	≈0.5(1)	9971.1					$15^- \longrightarrow 15^+$
1031.6	13.35(71)	6277.1	1.84(26)[h]		+0.094(35)	$E2$	$11^+ \longrightarrow 9^+$
1063.1	1.64(8)	6706.3					$\longrightarrow 10^+$
1076.8	2.58(11)	6720.0	1.92(22)[h]	1.14(13)	−0.080(68)	$E1$	$10^- \longrightarrow 10^+$
1108.0	6.62(41)	9971.1	0.66(7)[h]	0.43(9)	+0.059(57)	$M1+E2$	$15^- \longrightarrow 14^-$
1128.4[p]	43(3)	6374.8	1.06(2)[i]		+0.021(3)	$E1$	$10^- \longrightarrow 9^+$
1167.3	28.69(71)	10122.6	0.92(4)[f]	0.39(2)	+0.023(8)	$E1$	$16^- \rightarrow 15^+$
1233.4	4.36(25)	7025.1	0.88(10)[h]		−0.032(44)	$M1$	$10^+ \longrightarrow 9^+$
1277.5	8.10(35)	9333.5	0.78(7)[f]		−0.069(51)	$M1+E2$	$15^+ \longrightarrow 14^+$
1309.7	64(2)	6952.8		0.46(1)	+0.017(5)	$E1$	$11^- \longrightarrow 10^+$
1364.4	11.94(34)	7007.6	0.83(6)[h]	0.45(2)	+0.024(15)	$E1$	$11^- \longrightarrow 10^+$
1381.6	1.15(6)	7025.1	1.86(40)[h]	0.87(23)		$(E2)$[g]	$10^+ \longrightarrow 10^+$
1427.4	7.82(20)	8863.3	0.82(6)[h]	0.44(6)	+0.032(29)	$E1$	$14^- \longrightarrow 13^+$
1473.6	3.04(15)	6720.0	1.06(10)[h]		+0.032(45)	$E1$	$10^- \longrightarrow 9^+$
1519.9	≈0.5(1)	8955.1					$15^+ \longrightarrow 13^+$
1550.3	3.58(14)	7192.8	0.51(6)[h]		−0.005(78)	$M1+E2$	$11^+ \longrightarrow 10^+$
1554.5	<0.5	6720.0					$10^- \longrightarrow 8^+$
1574.9	3.08(10)	5164.3	1.36(19)[h]				$8^+ \longrightarrow 8^+$
1579.0	1.90(8)	7222.2	1.90(34)[h]	1.03(21)	+0.095(135)	$E2$	$12^+ \longrightarrow 10^+$
1641.3	1.79(9)	8863.3					$14^- \longrightarrow 12^+$
1658.1	73(2)	5246.4	1.43(3)[i]		−0.051(7)	$M1+E2$	$9^+ \longrightarrow 8^+$
1716.3	3.60(17)	5164.3	1.79(22)[h]		+0.073(93)	$E2$	$8^+ \longrightarrow 6^+$
1777.7	17.10(86)	9833.4	0.73(5)[f]	0.39(3)	+0.025(28)[q]	$E1$	$15^- \longrightarrow 14^+$
1778.9[r]	15(2)	7025.1					$10^+ \longrightarrow 9^+$
1807.0	<0.5	10761.7					$17^- \longrightarrow 15^+$
1861.1	3.32(19)	7025.1	2.23(25)[h]		+0.070(92)	$E2$	$10^+ \longrightarrow 8^+$
1898.1	6.39(20)	9333.5	1.59(20)[l]		+0.126(86)	$(E2)$[o]	$15^+ \longrightarrow 13^+$
1915.9	4.30(15)	9971.1	0.74(14)[h]		+0.036(58)	$E1$	$15^- \longrightarrow 14^+$
2054.7	100(2)	5643.2	2.01(6)[f]		+0.017(7)	$E2$	$10^+ \longrightarrow 8^+$
2202.8	18.53(54)	5791.5	0.99(5)[i]		−0.053(16)	$M1$	$9^+ \longrightarrow 8^+$
2398.0	<0.5	9833.4					$15^- \longrightarrow 13^+$
2688.7	6.60(22)	6277.1					$11^+ \longrightarrow 8^+$
3437.3	2.85(20)	7025.1	1.60(19)[h]			$(E2)$[o]	$10^+ \longrightarrow 8^+$

[a] The uncertainties of γ-ray energy centroids of strong ($I_\gamma \geqslant 15$) and weak ($I_\gamma < 15$) transitions are around 0.3 and 0.6 keV, respectively.

[b] Internal-conversion-corrected intensities of γ-ray transitions above the 8^+ state are normalized to the 2054.7-keV transition.

[c] R_{DCO} values are obtained using stretched dipole transitions as gate.

[d] R_{DCO} values are obtained using the 2054.7-keV gate (quadrupole transition).

[e] Not observed in this work, energy taken from Ref. [15].

[f] R_{DCO} values are obtained using the 1309.7-keV gate.

[g] Multipolarity assignment is based on the R_{DCO} measurements and the spin-parity of the initial and final levels. These spin-parity are determined from the measurements on other strong transitions.

[h] R_{DCO} values are obtained using the 213.3-keV gate. The mixing ratio of the 213.3-keV $M1$ transition is $\delta = +0.034^{+0.037}_{-0.042}$.

[i] R_{DCO} values are obtained using the 818.0-keV gate.

[j] Contains contributions from the 214.4-keV transition ($E_x = 7222.2$ keV, $12^+ \rightarrow 11^-$).

[k] For Δ_{asym} measurements, no strong transition as a gate is possible to eliminate contributions from the 213.3-keV transition ($E_x = 7435.6$ keV, $13^+ \rightarrow 12^+$). The R_{DCO} is measured for the unresolved (213.3 + 214.4)-keV transition.

[l] R_{DCO} values are obtained using the 269.4-keV gate.

[m] R_{DCO} and Δ_{asym} have contributions from another 429.3-keV transition ($E_x = 2748.1$ keV, $3^- \rightarrow 5^-$).

[n] R_{DCO} and Δ_{asym} are obtained for unresolved (637.4 + 638.3)-keV transition. The multipolarity assignments have been made on the basis of these values.

[o] The spin-parity of the initial and final levels of the marked transitions are determined from other strong transitions. R_{DCO} value is notably smaller compared with the expected value for stretched $E2$ transition indicating possible mixing of higher multipolarity, which needs further investigation. Multipolarity assignment has, therefore, been made tentative.

[p] The R_{DCO} and Δ_{asym} have contributions from another 1128.8-keV transition ($E_x = 3447.9$ keV, $6^+ \rightarrow 5^-$).

[q] Transitions parallel to the 1778.9-keV ($E_x = 7025.1$ keV, $10^+ \rightarrow 9^+$) transition are used as gate.

[r] For R_{DCO} and Δ_{asym} measurements, no strong transition as a gate is possible to eliminate contributions from the 1777.7-keV transition ($E_x = 9833.4$ keV, $15^- \rightarrow 14^+$).

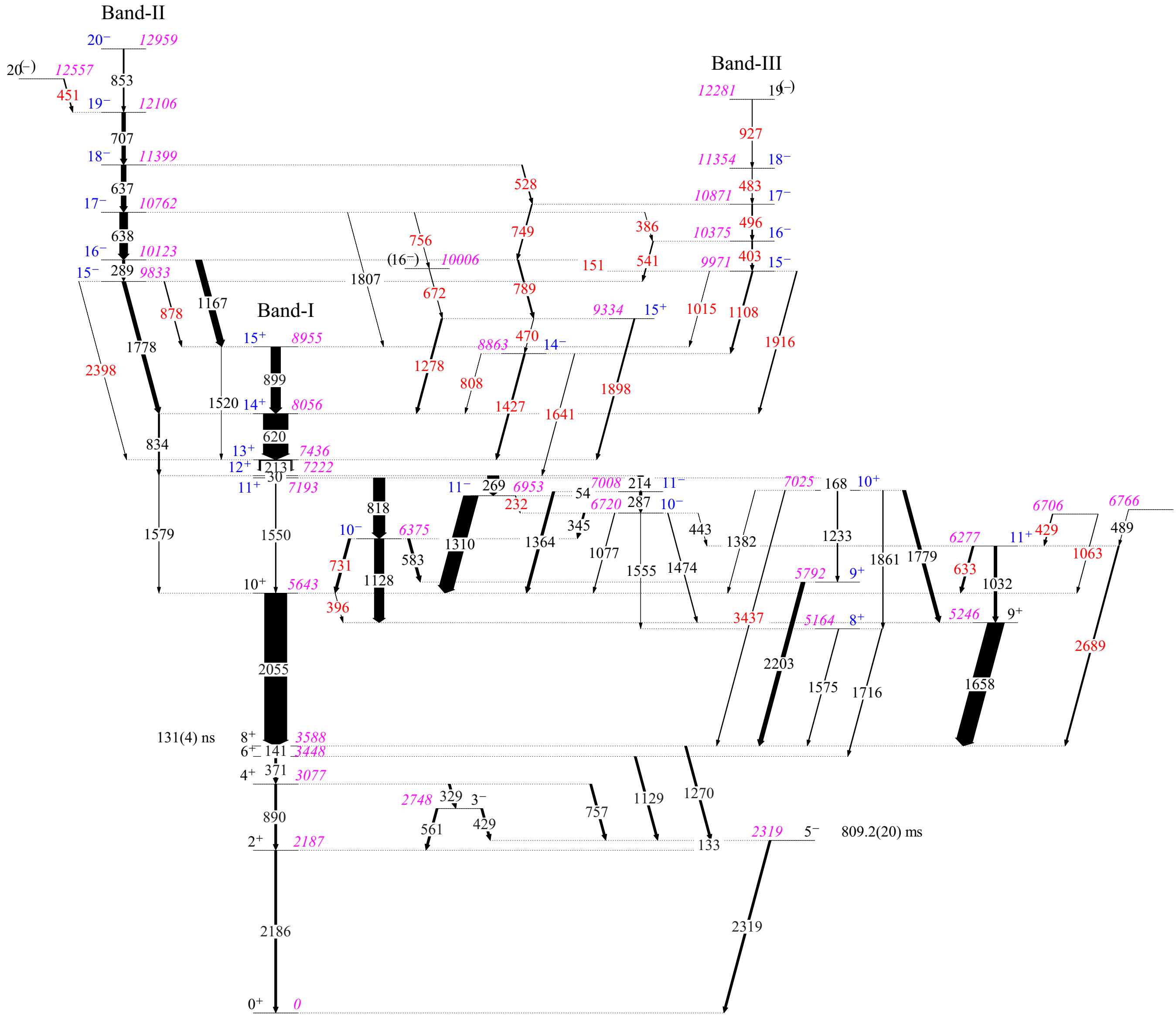

FIG. 1. Partial level scheme of ^{90}Zr developed in the present work. The energies of the excited states and γ-ray transitions are given in keV units. The thickness of the arrows above the 3588 keV state are proportional to the γ-ray intensities mentioned in Table I. Newly observed γ-ray transitions are marked by red labels. The spin-parity of the levels marked by blue labels have been measured. The purple labels represent the level energies in keV units. The experimentally observed values are given for γ-ray transition energies whereas the level energies are the output of the gamma-to-level (GTOL) least-squares fitting code developed at NNDC [44]. The transition energies and level energies shown in the level scheme have been rounded to the nearest whole numbers. The values of $t_{1/2}$ of the 2319 and 3588 keV levels are adopted from Ref. [45].

earlier work, too, where its parity was tentatively assigned as positive [15]. However, the new identification of the 899-keV transition of Band I as an $M1$ transition in conjunction with the confirmation of the 1167-keV transition, connecting the 10 123 keV level of the Band II to the 8955 keV 15^+ level of Band I, as an $E1$ transition, suggests that the parity of the band is negative. Further confirmation comes from the measurements of the 1778-keV transition, which is identified as an $E1$ transition. Although this identification is consistent with the polarization measurement done by Warburton *et al.*, which has a positive value (see Table III of Ref. [15]), the transition was ascribed as $M1$. Owing to the contaminations of the 1778-keV transition reported in Ref. [15], the multipolarity assignment for this transition was tentative in the previous work [15]. In the present study, the possibility of placing gates on specific transitions towards the measurement of the 1778-keV transition resolves this issue. In addition, we confirm the $M1$ assignment for the 638-, 637-, 707-, and 853-keV gamma transitions of the band (see Table I). Within the sensitivity limit of the present experiment, no crossover $E2$ transitions have been observed in this band. Levels of this band have also been observed to decay to the levels of Band I by multiple pathways. This includes the pathway via the newly identified levels at 8863, 9334, and 10 006 keV.

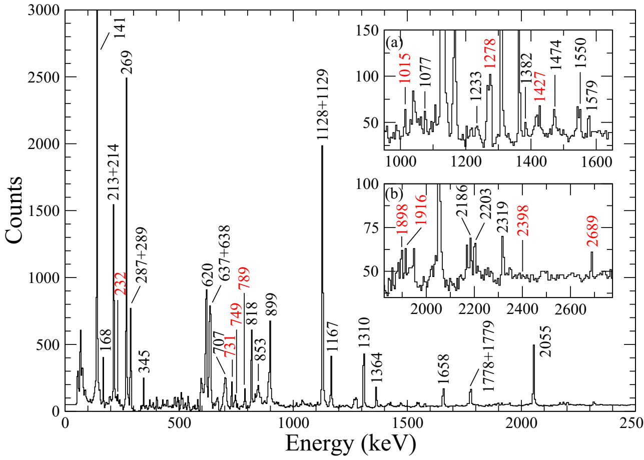

FIG. 2. Representative spectrum showing the sum of double-gated spectra with one gate on 213- and other on 620-, 1310-, 1658- and 2055-keV transitions. The newly observed transitions in ^{90}Zr are labeled in red. The insets (a) and (b) depict the expanded energy ranges from 950 to 1650 keV and from 1825 to 2775 keV, respectively.

In addition, two new transitions, viz. 878- and 2398-keV, are observed to decay from the 9833 keV 15^- level of the band to that of Band I.

C. Band III

A new level at $E_x = 8863$ keV has been observed which decays to the 7436 keV level through a 1427-keV transition. The results of R_{DCO} and Δ_{asym} measurements suggest an $E1$ multipolarity and thereby suggest the spin and parity of the level at 8863 keV as 14^-. This level is connected, via the 1108-keV transition of $M1 + E2$ type, to a new sequence of levels observed for the first time in this nucleus. Levels of this band have been determined as negative-parity levels connected by $M1$ transitions. However, the parity of the topmost level, decaying by a 927-keV transition, is kept tentative because Δ_{asym} could not be determined for this transition due to limited statistics. Some of these levels are also observed to be connected to the levels of Band I and Band II. Additionally, the polarization measurement of the 1916-keV transition, which suggests its $E1$ multipolarity, connecting to the 8056 keV level of Band I, provides further support to the negative-parity assignment of the levels of this band.

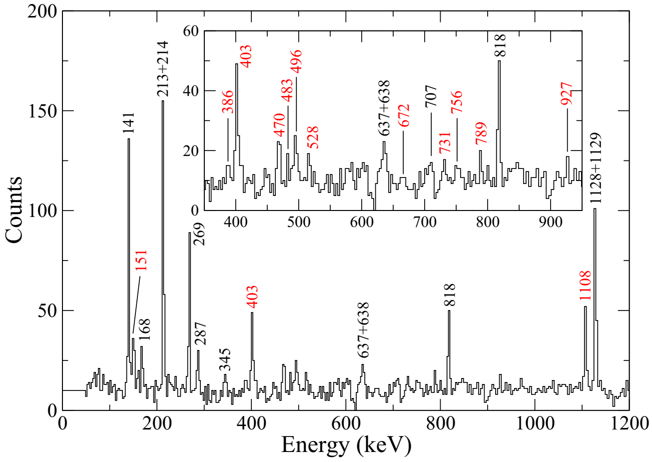

FIG. 3. Representative spectrum showing the sum of double-gated spectra with one gate on 1427- and other on 141-, 213-, 1310- and 2055-keV transitions. The newly observed transitions in ^{90}Zr are labeled in red. The inset shows the expanded energy range from 300 to 1000 keV for a better view of the weaker transitions.

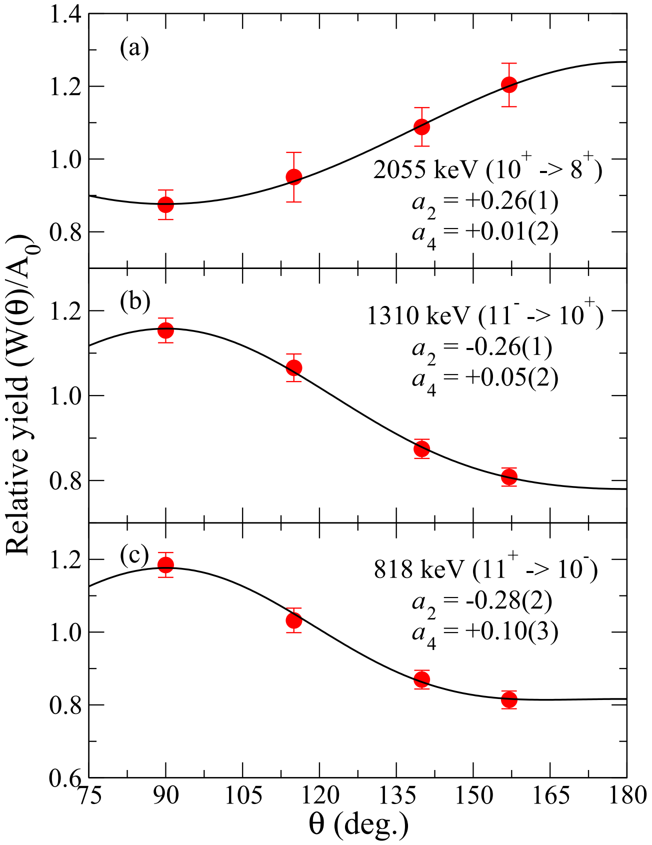

FIG. 4. Angular distribution of (a) $L = 2$, 2055-keV ($10^+ \rightarrow 8^+$); (b) $L = 1$, 1310-keV ($11^- \rightarrow 10^+$); and (c) $L = 1$, 818-keV ($11^+ \rightarrow 10^-$) γ-ray transitions in ^{90}Zr. The experimental data are represented by filled red circles and the fitted curve shown as a black solid line. The errors in relative yield have been multiplied by a factor of two for a better view.

D. Other states

In this group, levels at energies 5164, 5246, 5792, 6277, 6375, 6720, 6953, 7008, and 7025 keV are included. Most of the spin-parity assignments of the levels in this group were tentative before this work. These assignments are now confirmed through the DCO ratio and polarization measurements. Several new transitions of energies 232-, 396-, 633-, 731-, 2689-, and 3437-keV are added to the level scheme (see Fig. 1). However, no transition between the 7222 keV, 12^+ level of Band I and the 6277 keV, 11^+ level has been observed in this work. In addition, the 6766 keV level has been observed and a new level at 6706 keV excitation energy has been added. Due to the lack of statistics for the decay transitions from these levels, their the spin-parity assignments were not possible.

TABLE II. Major components of wave functions for positive-parity states in ^{90}Zr.

I^{π}	Probability	Proton	Neutron
$0^+_{\text{g.s.}}$	28.15%	$f_{5/2}^{6}p_{3/2}^{4}p_{1/2}^{0}g_{9/2}^{2}$	$g_{9/2}^{10}d_{5/2}^{0}$
	27.58%	$f_{5/2}^{6}p_{3/2}^{4}p_{1/2}^{2}g_{9/2}^{0}$	$g_{9/2}^{10}d_{5/2}^{0}$
2^+_1	38.57%	$f_{5/2}^{6}p_{3/2}^{4}p_{1/2}^{0}g_{9/2}^{2}$	$g_{9/2}^{10}d_{5/2}^{0}$
	16.53%	$f_{5/2}^{4}p_{3/2}^{4}p_{1/2}^{2}g_{9/2}^{2}$	$g_{9/2}^{10}d_{5/2}^{0}$
4^+_1	42.52%	$f_{5/2}^{6}p_{3/2}^{4}p_{1/2}^{0}g_{9/2}^{2}$	$g_{9/2}^{10}d_{5/2}^{0}$
	15.47%	$f_{5/2}^{4}p_{3/2}^{4}p_{1/2}^{2}g_{9/2}^{2}$	$g_{9/2}^{10}d_{5/2}^{0}$
6^+_1	50.76%	$f_{5/2}^{6}p_{3/2}^{4}p_{1/2}^{0}g_{9/2}^{2}$	$g_{9/2}^{10}d_{5/2}^{0}$
	13.90%	$f_{5/2}^{4}p_{3/2}^{4}p_{1/2}^{2}g_{9/2}^{2}$	$g_{9/2}^{10}d_{5/2}^{0}$
8^+_1	52.36%	$f_{5/2}^{6}p_{3/2}^{4}p_{1/2}^{0}g_{9/2}^{2}$	$g_{9/2}^{10}d_{5/2}^{0}$
	13.36%	$f_{5/2}^{4}p_{3/2}^{4}p_{1/2}^{2}g_{9/2}^{2}$	$g_{9/2}^{10}d_{5/2}^{0}$
8^+_2	40.89%	$f_{5/2}^{5}p_{3/2}^{4}p_{1/2}^{1}g_{9/2}^{2}$	$g_{9/2}^{10}d_{5/2}^{0}$
	20.68%	$f_{5/2}^{6}p_{3/2}^{3}p_{1/2}^{1}g_{9/2}^{2}$	$g_{9/2}^{10}d_{5/2}^{0}$
9^+_1	68.27%	$f_{5/2}^{5}p_{3/2}^{4}p_{1/2}^{1}g_{9/2}^{2}$	$g_{9/2}^{10}d_{5/2}^{0}$
	11.00%	$f_{5/2}^{5}p_{3/2}^{3}p_{1/2}^{2}g_{9/2}^{2}$	$g_{9/2}^{10}d_{5/2}^{0}$
9^+_2	37.59%	$f_{5/2}^{6}p_{3/2}^{3}p_{1/2}^{1}g_{9/2}^{2}$	$g_{9/2}^{10}d_{5/2}^{0}$
	24.10%	$f_{5/2}^{5}p_{3/2}^{4}p_{1/2}^{1}g_{9/2}^{2}$	$g_{9/2}^{10}d_{5/2}^{0}$
10^+_1	49.87%	$f_{5/2}^{6}p_{3/2}^{3}p_{1/2}^{1}g_{9/2}^{2}$	$g_{9/2}^{10}d_{5/2}^{0}$
	16.61%	$f_{5/2}^{5}p_{3/2}^{4}p_{1/2}^{1}g_{9/2}^{2}$	$g_{9/2}^{10}d_{5/2}^{0}$
10^+_2	67.01%	$f_{5/2}^{5}p_{3/2}^{4}p_{1/2}^{1}g_{9/2}^{2}$	$g_{9/2}^{10}d_{5/2}^{0}$
	9.68%	$f_{5/2}^{5}p_{3/2}^{3}p_{1/2}^{2}g_{9/2}^{2}$	$g_{9/2}^{10}d_{5/2}^{0}$
11^+_1	67.40%	$f_{5/2}^{5}p_{3/2}^{4}p_{1/2}^{1}g_{9/2}^{2}$	$g_{9/2}^{10}d_{5/2}^{0}$
	12.96%	$f_{5/2}^{5}p_{3/2}^{3}p_{1/2}^{2}g_{9/2}^{2}$	$g_{9/2}^{10}d_{5/2}^{0}$
11^+_2	33.69%	$f_{5/2}^{6}p_{3/2}^{4}p_{1/2}^{0}g_{9/2}^{2}$	$g_{9/2}^{9}d_{5/2}^{1}$
	18.27%	$f_{5/2}^{4}p_{3/2}^{4}p_{1/2}^{2}g_{9/2}^{2}$	$g_{9/2}^{9}d_{5/2}^{1}$
12^+_1	38.39%	$f_{5/2}^{6}p_{3/2}^{4}p_{1/2}^{0}g_{9/2}^{2}$	$g_{9/2}^{9}d_{5/2}^{1}$
	19.35%	$f_{5/2}^{4}p_{3/2}^{4}p_{1/2}^{2}g_{9/2}^{2}$	$g_{9/2}^{9}d_{5/2}^{1}$
13^+_1	41.41%	$f_{5/2}^{6}p_{3/2}^{4}p_{1/2}^{0}g_{9/2}^{2}$	$g_{9/2}^{9}d_{5/2}^{1}$
	19.26%	$f_{5/2}^{4}p_{3/2}^{4}p_{1/2}^{2}g_{9/2}^{2}$	$g_{9/2}^{9}d_{5/2}^{1}$
14^+_1	40.29%	$f_{5/2}^{6}p_{3/2}^{4}p_{1/2}^{0}g_{9/2}^{2}$	$g_{9/2}^{9}d_{5/2}^{1}$
	17.26%	$f_{5/2}^{4}p_{3/2}^{4}p_{1/2}^{2}g_{9/2}^{2}$	$g_{9/2}^{9}d_{5/2}^{1}$
15^+_1	27.58%	$f_{5/2}^{6}p_{3/2}^{4}p_{1/2}^{0}g_{9/2}^{2}$	$g_{9/2}^{9}d_{5/2}^{1}$
	25.24%	$f_{5/2}^{5}p_{3/2}^{4}p_{1/2}^{1}g_{9/2}^{2}$	$g_{9/2}^{9}d_{5/2}^{1}$
15^+_2	52.18%	$f_{5/2}^{5}p_{3/2}^{4}p_{1/2}^{1}g_{9/2}^{2}$	$g_{9/2}^{9}d_{5/2}^{1}$
	16.24%	$f_{5/2}^{6}p_{3/2}^{4}p_{1/2}^{0}g_{9/2}^{2}$	$g_{9/2}^{9}d_{5/2}^{1}$

IV. THEORETICAL CALCULATIONS AND DISCUSSION

^{90}Zr has $Z = 40$ and $N = 50$, making it a semimagic nucleus. As a consequence, the structure of its low-lying states displays characteristic features of a spherical nucleus, *i.e.*, they are described quite successfully within the scope of the shell model with a spherical mean field. Even at the high-spin and excitation energies, observed so far, the absence of strong $E2$ transitions suggests no appreciable collectivity.

Early shell-model calculations for ^{90}Zr were performed with a smaller model space, where protons were restricted to the $1f_{5/2}, 2p_{3/2}, 2p_{1/2}, 1g_{9/2}$ orbitals, while the neutron $2p_{1/2}$, $1g_{9/2}$ orbitals were completely filled [1]. In a later study, it is shown to be necessary to include the neutron orbitals above the $N = 50$ shell gap in the model space for the description of states with spin $I > 12\hbar$, although good agreement with experimental data is reported for states below $I = 12\hbar$ [15,48]. High-spin states in many nuclei in this mass region viz. ^{86}Kr [2], ^{88}Kr [3], ^{87}Rb [4], ^{89}Rb [3], ^{88}Sr [6], ^{89,90}Sr [7], ^{89}Y [11,12], ^{90}Y [13], ^{91}Y [14], ^{91,92}Zr [18], ^{91}Nb [21], ^{92}Mo [23], ^{93}Mo [24], ^{94}Mo [25], ^{93}Tc [27], ^{94}Tc [28], ^{94}Ru [29], ^{95}Ru [30], and ^{95}Rh [31] have been studied using the extended model space with the inclusion of neutron orbitals above $N = 50$ shell gap.

A. Shell-model calculations

To interpret the experimental data, we have performed shell-model calculations using the GWBXG effective interaction with the ^{68}Ni core. The GWBXG interaction has $1f_{5/2}$, $2p_{3/2}$, $2p_{1/2}$, $1g_{9/2}$ proton orbitals and $2p_{1/2}$, $1g_{9/2}$, $1g_{7/2}$, $2d_{5/2}$, $2d_{3/2}$, and $3s_{1/2}$ neutron orbitals. The single-particle energies (in MeV) used in this interaction are $1f_{5/2} = -5.322$, $2p_{3/2} = -6.144$, $2p_{1/2} = -3.941$, $1g_{9/2} = -1.250$ for the proton orbitals, and $2p_{1/2} = -0.696$, $1g_{9/2} = -2.597$, $1g_{7/2} = +5.159$, $2d_{5/2} = +1.830$, $2d_{3/2} = +4.261$, $3s_{1/2} = +1.741$ for the neutron orbitals. In our calculations for the neutrons we have completely filled $2p_{1/2}$, while we have not allowed any neutrons to occupy the $1g_{7/2}$ and $2d_{3/2}$ orbitals. Furthermore, since the dimension is very large, we have allowed a maximum of one neutron each in the $2d_{5/2}$ and $3s_{1/2}$ orbitals. Calculations are performed with the shell-model code KSHELL [49]. The GWBXG effective interaction is constructed with different interactions. The original 974 two-body matrix elements (TBMEs) are obtained from bare G matrix of the H7B potential [50]. The bare G matrix is not reasonable because of the space truncation and the interaction should be renormalized by taking into account the core-polarization effects. Here, the present G-matrix effective interaction is further tuned by modifying matrix elements with fit interactions as follows: The 65 TBMEs for proton orbitals are replaced with the effective values reported in Ref. [51]. The TBMEs connecting the $\pi(2p_{1/2}, 1g_{9/2})$ and the $\nu(2d_{5/2}, 3s_{1/2})$ orbitals are replaced by those from the work of Gloeckner [52]. The TBMEs between the $\pi(2p_{1/2}, 1g_{9/2})$ and the $\nu(2p_{1/2}, 1g_{9/2})$ orbitals are replaced with the values determined by Serduke *et al.* [53]. Earlier, shell-model results for high-spin states of ^{91}Y and ^{95}Nb using this interaction have been reported in Ref. [14]. Also, the positive-parity yrast states of the neutron-rich ^{89}Rb, ^{92}Y, and ^{93}Y nuclei using the same interaction have been reported in Ref. [54].

The calculated results for spin up to $I = 15\hbar$ and excitation energy of around 9 MeV for positive-parity states, while $I = 20\hbar$ and excitation energy of around 13 MeV for negative-parity states are presented in Tables II and III, respectively. The percentage contributions of the first two dominant configurations of the corresponding states spanning the experimentally observed range are also listed there. Comparison with experimental results for level energies are shown in Figs. 5 and 6 for positive-parity and negative-parity states, respectively. It is important to mention here that, between the 8^+_1 and 8^+_2, 11^+_1 and 11^+_2, and 14^+_1 and 15^+_1 states, one gets several states in shell-model calculations, but we have shown

TABLE III. Major components of wave functions for negative-parity states in ^{90}Zr.

I^π	Probability	Proton	Neutron
3_1^-	60.40%	$f_{5/2}^{6}p_{3/2}^{3}p_{1/2}^{2}g_{9/2}^{1}$	$g_{9/2}^{10}d_{5/2}^{0}$
	10.86%	$f_{5/2}^{6}p_{3/2}^{3}p_{1/2}^{0}g_{9/2}^{3}$	$g_{9/2}^{10}d_{5/2}^{0}$
5_1^-	74.56%	$f_{5/2}^{6}p_{3/2}^{4}p_{1/2}^{1}g_{9/2}^{1}$	$g_{9/2}^{10}d_{5/2}^{0}$
	9.93%	$f_{5/2}^{6}p_{3/2}^{2}p_{1/2}^{1}g_{9/2}^{3}$	$g_{9/2}^{10}d_{5/2}^{0}$
10_1^-	68.21%	$f_{5/2}^{5}p_{3/2}^{4}p_{1/2}^{0}g_{9/2}^{3}$	$g_{9/2}^{10}d_{5/2}^{0}$
	10.54%	$f_{5/2}^{5}p_{3/2}^{3}p_{1/2}^{1}g_{9/2}^{3}$	$g_{9/2}^{10}d_{5/2}^{0}$
10_2^-	32.79%	$f_{5/2}^{5}p_{3/2}^{4}p_{1/2}^{0}g_{9/2}^{3}$	$g_{9/2}^{10}d_{5/2}^{0}$
	21.01%	$f_{5/2}^{4}p_{3/2}^{4}p_{1/2}^{1}g_{9/2}^{3}$	$g_{9/2}^{10}d_{5/2}^{0}$
11_1^-	60.93%	$f_{5/2}^{5}p_{3/2}^{4}p_{1/2}^{0}g_{9/2}^{3}$	$g_{9/2}^{10}d_{5/2}^{0}$
	11.81%	$f_{5/2}^{5}p_{3/2}^{3}p_{1/2}^{1}g_{9/2}^{3}$	$g_{9/2}^{10}d_{5/2}^{0}$
11_2^-	33.50%	$f_{5/2}^{4}p_{3/2}^{4}p_{1/2}^{1}g_{9/2}^{3}$	$g_{9/2}^{10}d_{5/2}^{0}$
	17.08%	$f_{5/2}^{5}p_{3/2}^{4}p_{1/2}^{0}g_{9/2}^{3}$	$g_{9/2}^{10}d_{5/2}^{0}$
14_1^-	49.70%	$f_{5/2}^{5}p_{3/2}^{4}p_{1/2}^{0}g_{9/2}^{3}$	$g_{9/2}^{9}d_{5/2}^{1}$
	10.77%	$f_{5/2}^{5}p_{3/2}^{3}p_{1/2}^{1}g_{9/2}^{3}$	$g_{9/2}^{9}d_{5/2}^{1}$
15_1^-	43.82%	$f_{5/2}^{4}p_{3/2}^{4}p_{1/2}^{1}g_{9/2}^{3}$	$g_{9/2}^{10}d_{5/2}^{0}$
	30.80%	$f_{5/2}^{5}p_{3/2}^{3}p_{1/2}^{1}g_{9/2}^{3}$	$g_{9/2}^{10}d_{5/2}^{0}$
15_2^-	36.23%	$f_{5/2}^{5}p_{3/2}^{4}p_{1/2}^{0}g_{9/2}^{3}$	$g_{9/2}^{9}d_{5/2}^{1}$
	27.48%	$f_{5/2}^{5}p_{3/2}^{4}p_{1/2}^{0}g_{9/2}^{3}$	$g_{9/2}^{9}s_{1/2}^{1}$
16_1^-	52.93%	$f_{5/2}^{5}p_{3/2}^{4}p_{1/2}^{0}g_{9/2}^{3}$	$g_{9/2}^{9}d_{5/2}^{1}$
	13.26%	$f_{5/2}^{5}p_{3/2}^{3}p_{1/2}^{1}g_{9/2}^{3}$	$g_{9/2}^{9}d_{5/2}^{1}$
16_2^-	29.93%	$f_{5/2}^{5}p_{3/2}^{3}p_{1/2}^{1}g_{9/2}^{3}$	$g_{9/2}^{9}d_{5/2}^{1}$
	27.79%	$f_{5/2}^{5}p_{3/2}^{4}p_{1/2}^{0}g_{9/2}^{3}$	$g_{9/2}^{9}d_{5/2}^{1}$
16_3^-	30.57%	$f_{5/2}^{5}p_{3/2}^{4}p_{1/2}^{0}g_{9/2}^{3}$	$g_{9/2}^{9}d_{5/2}^{1}$
	24.06%	$f_{5/2}^{4}p_{3/2}^{4}p_{1/2}^{1}g_{9/2}^{3}$	$g_{9/2}^{9}d_{5/2}^{1}$
17_1^-	57.68%	$f_{5/2}^{5}p_{3/2}^{4}p_{1/2}^{0}g_{9/2}^{3}$	$g_{9/2}^{9}d_{5/2}^{1}$
	14.92%	$f_{5/2}^{5}p_{3/2}^{3}p_{1/2}^{1}g_{9/2}^{3}$	$g_{9/2}^{9}d_{5/2}^{1}$
17_2^-	33.32%	$f_{5/2}^{5}p_{3/2}^{4}p_{1/2}^{0}g_{9/2}^{3}$	$g_{9/2}^{9}d_{5/2}^{1}$
	20.77%	$f_{5/2}^{4}p_{3/2}^{4}p_{1/2}^{1}g_{9/2}^{3}$	$g_{9/2}^{9}d_{5/2}^{1}$
18_1^-	55.84%	$f_{5/2}^{5}p_{3/2}^{4}p_{1/2}^{0}g_{9/2}^{3}$	$g_{9/2}^{9}d_{5/2}^{1}$
	16.66%	$f_{5/2}^{5}p_{3/2}^{3}p_{1/2}^{1}g_{9/2}^{3}$	$g_{9/2}^{9}d_{5/2}^{1}$
18_2^-	56.12%	$f_{5/2}^{5}p_{3/2}^{3}p_{1/2}^{1}g_{9/2}^{3}$	$g_{9/2}^{9}d_{5/2}^{1}$
	14.01%	$f_{5/2}^{4}p_{3/2}^{4}p_{1/2}^{1}g_{9/2}^{3}$	$g_{9/2}^{9}d_{5/2}^{1}$
19_1^-	59.41%	$f_{5/2}^{5}p_{3/2}^{4}p_{1/2}^{0}g_{9/2}^{3}$	$g_{9/2}^{9}d_{5/2}^{1}$
	14.57%	$f_{5/2}^{5}p_{3/2}^{3}p_{1/2}^{1}g_{9/2}^{3}$	$g_{9/2}^{9}d_{5/2}^{1}$
19_2^-	57.35%	$f_{5/2}^{5}p_{3/2}^{3}p_{1/2}^{1}g_{9/2}^{3}$	$g_{9/2}^{9}d_{5/2}^{1}$
	18.71%	$f_{5/2}^{4}p_{3/2}^{4}p_{1/2}^{1}g_{9/2}^{3}$	$g_{9/2}^{9}d_{5/2}^{1}$
20_1^-	61.50%	$f_{5/2}^{5}p_{3/2}^{4}p_{1/2}^{0}g_{9/2}^{3}$	$g_{9/2}^{9}d_{5/2}^{1}$
	11.79%	$f_{5/2}^{5}p_{3/2}^{3}p_{1/2}^{1}g_{9/2}^{3}$	$g_{9/2}^{9}d_{5/2}^{1}$
20_2^-	51.04%	$f_{5/2}^{5}p_{3/2}^{3}p_{1/2}^{1}g_{9/2}^{3}$	$g_{9/2}^{9}d_{5/2}^{1}$
	27.88%	$f_{5/2}^{4}p_{3/2}^{4}p_{1/2}^{1}g_{9/2}^{3}$	$g_{9/2}^{9}d_{5/2}^{1}$

only states for comparison with the experimental data. The same holds for the negative-parity states as well.

B. Low-spin states

TABLE IV. Shell-model results for average occupancy of different orbitals for different states.

I^π	$\pi[1f_{5/2}]$	$\pi[2p_{3/2}]$	$\pi[2p_{1/2}]$	$\pi[1g_{9/2}]$	$\nu[1g_{9/2}]$	$\nu[2d_{5/2}]$	$\nu[3s_{1/2}]$
$0^+_{\text{g.s.}}$	5.702	3.408	1.230	1.660	9.940	0.056	0.004
2_1^+	5.329	3.592	0.848	2.231	9.865	0.129	0.006
4_1^+	5.395	3.582	0.820	2.203	9.879	0.114	0.007
6_1^+	5.538	3.524	0.753	2.185	9.912	0.082	0.006
8_1^+	5.541	3.615	0.675	2.169	9.906	0.090	0.004
8_2^+	5.265	3.458	1.121	2.155	9.861	0.133	0.006
9_1^+	5.052	3.668	1.126	2.154	9.932	0.061	0.007
9_2^+	5.415	3.269	1.180	2.135	9.843	0.151	0.006
10_1^+	5.500	3.089	1.243	2.169	9.903	0.091	0.006
10_2^+	5.023	3.666	1.138	2.173	9.924	0.071	0.006
11_1^+	4.949	3.632	1.152	2.267	9.942	0.051	0.007
11_2^+	5.367	3.572	0.918	2.143	8.995	0.875	0.136
12_1^+	5.381	3.562	0.921	2.137	8.995	0.968	0.026
13_1^+	5.402	3.565	0.898	2.135	8.995	0.988	0.017
14_1^+	5.407	3.561	0.890	2.142	8.996	0.996	0.008
15_1^+	5.273	3.533	1.039	2.155	8.995	0.984	0.021
15_2^+	5.128	3.680	1.022	2.170	8.995	0.974	0.030
3_1^-	5.774	2.929	1.662	1.635	9.951	0.043	0.005
5_1^-	5.907	3.682	1.091	1.320	9.959	0.039	0.002
10_1^-	4.890	3.722	0.321	3.067	9.910	0.078	0.012
10_2^-	4.752	3.530	0.656	3.062	9.893	0.095	0.012
11_1^-	4.838	3.706	0.390	3.066	9.899	0.089	0.012
11_2^-	4.718	3.434	0.804	3.044	9.886	0.103	0.012
14_1^-	4.790	3.674	0.476	3.060	9.002	0.843	0.155
15_1^-	4.442	3.369	1.125	3.064	9.893	0.094	0.013
15_2^-	4.814	3.713	0.408	3.065	8.975	0.624	0.401
16_1^-	4.825	3.672	0.444	3.060	8.988	0.864	0.148
16_2^-	4.712	3.437	0.800	3.050	8.991	0.921	0.088
16_3^-	4.574	3.600	0.778	3.048	8.989	0.915	0.096
17_1^-	4.820	3.669	0.452	3.059	8.993	0.936	0.071
17_2^-	4.636	3.625	0.681	3.058	8.989	0.866	0.145
18_1^-	4.783	3.673	0.483	3.062	8.994	0.961	0.045
18_2^-	4.787	3.078	1.102	3.033	8.991	0.938	0.071
19_1^-	4.773	3.678	0.477	3.072	8.996	0.997	0.007
19_2^-	4.732	3.128	1.105	3.035	8.993	0.962	0.045
20_1^-	4.769	3.686	0.463	3.082	8.996	0.998	0.006
20_2^-	4.640	3.178	1.144	3.038	8.992	0.953	0.055

Calculated excitation energies for the low-lying states up to 7 MeV for both parities are in reasonable agreement with the experimental energies. These results can be compared with those reported earlier [15], where the difference between the observed and the calculated level energies was on average 320 keV, in contrast with around 270 keV in the present work. The major contribution towards the structure of positive-parity states comes from the configuration with proton excitations across the $Z = 40$ subshell gap, i.e., $\pi[(1f_{5/2}2p)^{-2}(1g_{9/2})^2]$. For negative-parity states, the contributions come mainly from the $\pi[(2p)^{-1}(1g_{9/2})^1]$ and $\pi[(1f_{5/2}2p)^{-3}(1g_{9/2})^3]$ configurations. The calculated 2_1^+-4_1^+-6_1^+-8_1^+ states arise from breaking one proton pair in the $g_{9/2}$ orbital; these states have seniority $v = 2$. The seniority of the 8_2^+, 9_1^+, and 10_1^+ states is four because there is one hole in $\pi[1f_{5/2}]$, another hole in $\pi[2p_{1/2}]$, and they couple with the breaking of a pair in $1g_{9/2}$. The seniority of the 3_1^- and 5_1^- states is two; these states result from the coupling of one proton hole in $p_{3/2}/p_{1/2}$ and one proton particle in $g_{9/2}$.

C. High-spin states

The configurations used by Warburton *et al.* to describe experimental high-spin states were $\pi[(1f_{5/2}2p)^{-n}(1g_{9/2})^n]$, where $n = 2, 4$ and $n = 1, 3$ for positive- and negative-

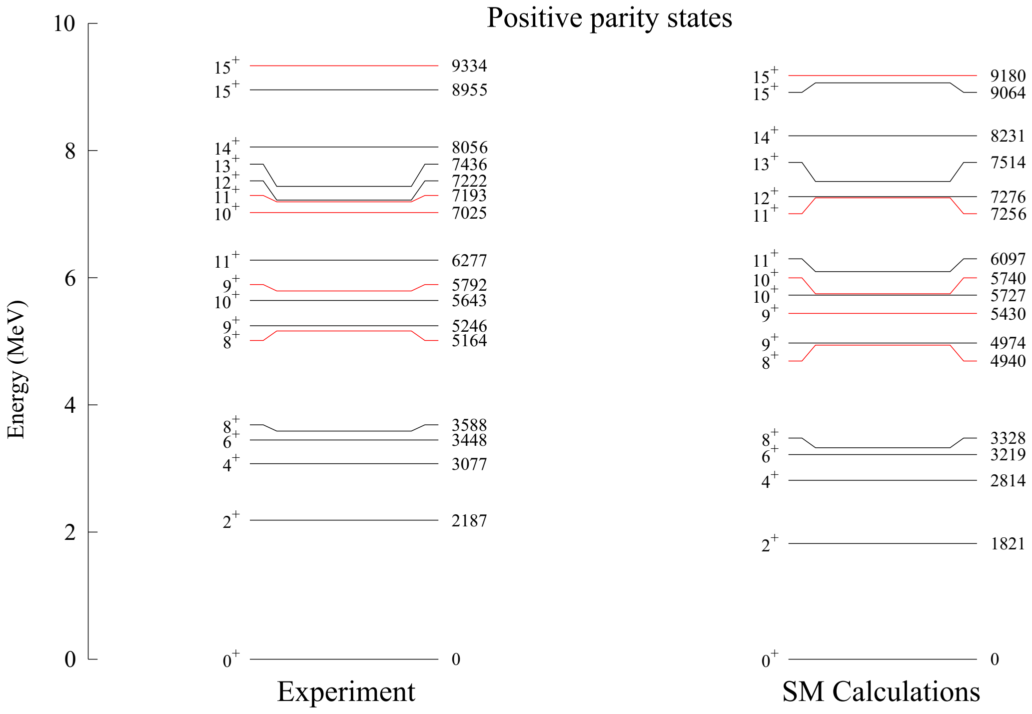

FIG. 5. A comparison of the experimental excitation energies of the positive-parity states (left) of ^{90}Zr with those from shell-model calculations using the GWBXG effective interaction (right). For a given spin whenever more than one state is present, they have been marked with red (second-excited state).

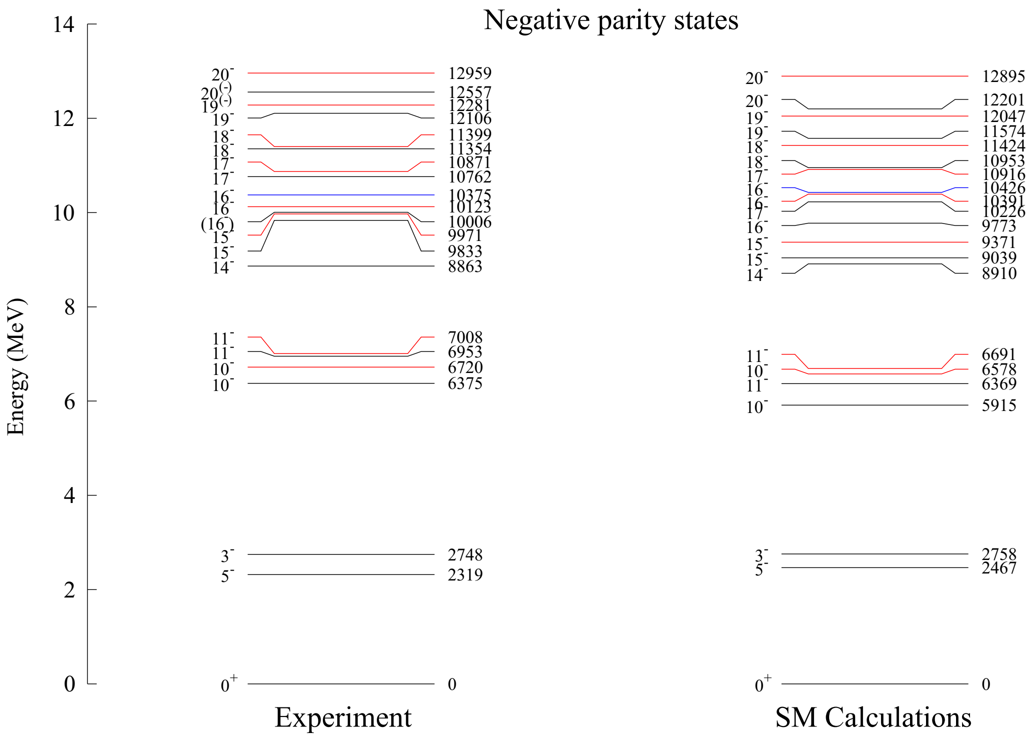

FIG. 6. A comparison of the experimental excitation energies of the negative-parity states (left) of ^{90}Zr with those from shell-model calculations using the GWBXG effective interaction (right). For a given spin, whenever more than one state is present, they have been marked with red (second-excited state) and blue (third-excited state).

parity states, respectively [15]. To generate more spin, neutron excitations were also allowed, but the calculated levels were not mentioned in Ref. [15]. Although the calculations reproduced the experimental energy levels fairly well, the calculated 12^+ level in this model space was predicted at 7784 keV, which was ≈550 keV higher than the experimental value. On the other hand, the present calculations predict a sequence of levels—11_2^+, 12_1^+, 13_1^+, 14_1^+, and 15_1^+—at 7256, 7276, 7514, 8231, and 9064 keV excitation energy, respectively (see Fig. 5), having the dominant configurations $\pi[(1g_{9/2})^2]_{8^+} \otimes \nu[(1g_{9/2})^{-1}(2d_{5/2})^1]_{7^+}$ and $\pi[(1f_{5/2})^{-2}(1g_{9/2})^2]_{12^+} \otimes \nu[(1g_{9/2})^{-1}(2d_{5/2})^1]_{7^+}$ with enhanced $M1$ transitions between them. An 11_1^+ level has been predicted at 6097 keV, which has $\pi[(1f_{5/2})^{-1}(2p)^{-1}(1g_{9/2})^2]$ as the most dominant configuration. One can see that the configurations of the levels of the aforementioned sequence have neutron-excited structures from $1g_{9/2}$ to $2d_{5/2}$ orbital, which is completely different from the configuration of the 11_1^+ level. As mentioned earlier, no γ-ray transition has been observed experimentally from the 12_1^+ to the 11_1^+ level due to their structural differences. The seniority of the configurations of the levels of Band I is four. The calculated $B(M1)$ strengths of ≈1 W.u. of the transitions of the band are also in reasonable agreement with the experimentally observed values [15]. A noticeable feature of the structure of these states is the coupling of protons and neutrons among themselves in an almost stretched configuration, which then recouple to form states of different total spin. The fully aligned $\pi[(1g_{9/2})^2]_{8^+}$ structure with spin-parity of 8^+ is observed at an excitation energy of 3588 keV. The coupling of this proton structure with the neutron-core excited structure $\nu[(1g_{9/2})^{-1}(2d_{5/2})^1]_{7^+}$ forms the states of Band I. Note that the sequence starts at an excitation energy 3.6 MeV higher than the fully aligned proton structure. This indicates the simultaneous excitations of protons and neutrons across the $Z = 40$ and $N = 50$ shell gaps, respectively. Similar excitations have been observed in ^{88}Sr around 9 MeV identified as the 13^+ state and above for the positive-parity band by Stefanova *et al.* [6]. In their work, the calculated 12_3^+, 13_1^+, 14_1^+, 15_1^+, and 16_1^+ states have this configuration. Such a scenario is also observed in ^{91,92}Zr, where the states with neutron-core excited configuration lie at ≈4–4.5 MeV higher in excitation energy than the corresponding unexcited neutron configurations [18]. In ^{91}Zr, the $21/2^+$ state having the fully aligned $\pi[(1g_{9/2})^2]_{8^+} \otimes \nu[(2d_{5/2})^1]_{5/2^+}$ configuration is observed at 3166 keV excitation energy. This configuration couples to the aforementioned neutron-core excited configuration to form a sequence at ≈7 MeV excitation energy starting with the $27/2^+$ state. In ^{92}Zr, the states above the $I^\pi = (17^+)$ lying at ≈9.6 MeV excitation energy correspond to the coupling of the neutron core excitation structure and the fully aligned (12^+) state at 4948 keV.

For negative-parity states with spin higher than $I = 15\hbar$, an additional excitation of proton across the $Z = 40$ subshell to the $g_{9/2}$ orbital is required. Therefore, the following configurations are suggested to form the dominant part of the structure of the states of negative-parity Band II and Band III: $\pi[(1f_{5/2})^{-1}(2p_{1/2})^{-2}(1g_{9/2})^3] \otimes \nu[(1g_{9/2})^{-1}(2d_{5/2})^1]$, $\pi[(1f_{5/2})^{-2}(2p_{1/2})^{-1}(1g_{9/2})^3] \otimes \nu[(1g_{9/2})^{-1}(2d_{5/2})^1]$, and $\pi[(1f_{5/2})^{-1}(2p_{3/2})^{-1}(2p_{1/2})^{-1}(1g_{9/2})^3] \otimes \nu[(1g_{9/2})^{-1}(2d_{5/2})^1]$. These configurations have seniority ranging from $v = 4$ to 6. Similar to Band I, the high-spin states in these bands are generated by the recoupling of nearly stretched proton and neutron configurations.

The configuration with neutron particle-hole excitation across the $N = 50$ shell gap has been observed to be a major component of the structure of high-spin yrast states of nuclei in this mass region [6,8,16,17,33]. This is because of the role of an additional neutron hole in the $g_{9/2}$ orbital in contributing to the spin of these yrast states. These high-spin states form a band-like structure with enhanced $M1$ transitions, similar to what has been observed in ^{90}Zr. As mentioned above, these configurations have stretched proton and neutron configurations, and high spin is generated by their recoupling.

In Table IV, we have shown the average occupancy of different orbitals corresponding to different states. The occupancy of $\nu[3s_{1/2}]$ and $\nu[2d_{5/2}]$ orbitals are increasing with spin. It reflects the importance of the inclusion of neutron orbitals beyond the $N = 50$ shell for high-spin states.

V. SUMMARY

The level scheme of ^{90}Zr has been substantially extended with the addition of thirty-two new transitions. The spin-parity of different states up to spin $20\hbar$ and excitation energy ≈13 MeV have been established on the basis of angular distribution, angular correlation, and polarization measurements. One of the important features of the present level scheme is the presence of two $\Delta I = 1$, $M1$ sequences at higher spins. The shell-model calculations, with the extended model space including neutron excitations across the $N = 50$ shell gap, give a good description of both the positive- as well as the negative-parity states up to highest observed excitation energy and spin. This indicates the dominance of single-particle excitations in this nucleus. The role of occupancy of neutrons in $2d_{5/2}$ and $3s_{1/2}$ beyond the $N = 50$ shell gap for the description of high-spin states has been highlighted.

ACKNOWLEDGMENTS

The authors are grateful to the staff at TIFR-BARC Pelletron Linac Facility for providing a good-quality beam and smooth operation of the accelerator for the entire duration of the experiment. The help and cooperation from B. Naidu, S. Jadhav, A. T. Vazhappilly, and R. Donthi in setting the experiment is acknowledged. This work is supported by the Department of Atomic Energy, Government of India (Project Identification Code: 12-R&D-TFR-5.02-0200) and the Department of Science and Technology, Government of India (Grant No. IR/S2/PF-03/2003-II). R.P. and E.I. acknowledge the RCNP Collaboration Research network (COREnet) program. E.I. acknowledges the support by the International Joint Research Promotion Program of Osaka University and JSPS KAKENHI Grant No. JP17H02893. U.G. acknowledges the U. S. National Science Foundation (Grant No. PHY-2011890). D.N. would like to acknowledge the financial support from the CSIR, India towards this project. P.C.S. acknowledges a research grant from SERB (India), CRG/2019/000556.

[1] H. C. Chiang, M. C. Wang, and C. S. Han, J. Phys. G: Nucl. Phys. **6**, 345 (1980).

[2] G. Winter, R. Schwengner, J. Reif, H. Prade, L. Funke, R. Wirowski, N. Nicolay, A. Dewald, P. von Brentano, H. Grawe, and R. Schubart, Phys. Rev. C **48**, 1010 (1993).

[3] A. Astier, M.-G. Porquet, Ts. Venkova, G. Duchêne, F. Azaiez, D. Curien, I. Deloncle, O. Dorvaux, B. J. P. Gall, N. Redon, M. Rousseau, and O. Stézowski, Phys. Rev. C **88**, 024321 (2013).

[4] L. Käubler, K. D. Schilling, R. Schwengner, F. Dönau, E. Grosse, D. Belic, P. von Brentano, M. Bubner, C. Fransen, M. Grinberg, U. Kneissl, C. Kohstall, A. Linnemann, P. Matschinsky, A. Nord, N. Pietralla, H. H. Pitz, M. Scheck, F. Stedile, and V. Werner, Phys. Rev. C **65**, 054315 (2002).

[5] J. J. Liu, Y. Zheng, H. B. Sun, X. G. Wu, C. Y. He, G. S. Li, C. B. Li, S. H. Yao, H. W. Li, S. P. Hu, J. L. Wang, W. W. Qu, C. Xu, and J. J. Sun, Eur. Phys. J. A **50**, 84 (2014).

[6] E. A. Stefanova, R. Schwengner, J. Reif, H. Schnare, F. Dönau, M. Wilheim, M. Wilhelm, A. Fitzler, S. S. Kasemann, P. von Brentano, and W. Andrejtscheff, Phys. Rev. C **62**, 054314 (2000).

[7] E. A. Stefanova, R. Schwengner, G. Rainovski, K. D. Schilling, A. Wagner, F. Dönau, E. Galindo, A. Jungclaus, K. P. Lieb, O. Thelen, J. Eberth, D. R. Napoli, C. A. Ur, G. de Angelis, M. Axiotis, A. Gadea, N. Marginean, T. Martinez, Th. Kröll, and T. Kutsarova, Phys. Rev. C **63**, 064315 (2001).

[8] R. Schwengner, J. Reif, H. Schnare, G. Winter, T. Servene, L. Käubler, H. Prade, M. Wilhelm, A. Fitzler, S. Kasemann, E. Radermacher, and P. von Brentano, Phys. Rev. C **57**, 2892 (1998).

[9] C. J. Xu, S. Y. Wang, C. Y. Niu, C. Liu, B. Qi, D. P. Sun, L. Liu, P. Zhang, Z. Q. Li, Z. Wang, X. G. Wu, G. S. Li, C. Y. He, Y. Zheng, B. B. Yu, C. B. Li, S. P. Hu, S. H. Yao, X. P. Cao, J. L. Wang *et al.*, Phys. Rev. C **86**, 027302 (2012).

[10] M. Bunce, P. H. Regan, V. Werner, C. W. Beausang, V. Anagnostatou, M. Bowry, R. J. Casperson, D. Chen, N. Cooper, P. M. Goddard, R. O. Hughes, G. Ilie, P. J. R. Mason, B. Pauerstein, M. W. Reed, T. J. Ross, and E. C. Simpson, Phys. Rev. C **87**, 044337 (2013).

[11] L. Funke, G. Winter, J. Döring, L. Käubler, H. Prade, R. Schwengner, E. Will, Ch. Protochristov, W. Andrejtschef, L. G. Kostova, P. O. Lipas, and R. Wirowski, Nucl. Phys. A **541**, 241 (1992).

[12] J. Reif, G. Winter, L. Käubler, H. Prade, and R. Schwengner, Nucl. Phys. A **587**, 449 (1995).

[13] G. Rainovski, R. Schwengner, K. D. Schilling, A. Wagner, A. Jungclaus, E. Galindo, O. Thelen, D. R. Napoli, C. A. Ur, G. de Angelis, M. Axiotis, A. Gadea, N. Marginean, T. Martinez, and Th. Kröll, Phys. Rev. C **65**, 044327 (2002).

[14] D. Bucurescu, Zs. Podolyák, C. Rusu, G. de Angelis, Y. H. Zhang, G. Căta-Danil, I. Căta-Danil, M. Ivaşcu, N. Mărginean, R. Mărginean, L. C. Mihăilescu, G. A. Suliman, P. H. Regan, W. Gelletly, S. D. Langdown, J. J. Valiente Dobón, D. Bazzacco, S. Lunardi, C. A. Ur, M. Axiotis *et al.*, Phys. Rev. C **71**, 034315 (2005).

[15] E. K. Warburton, J. W. Olness, C. J. Lister, R. W. Zurmühle, and J. A. Becker, Phys. Rev. C **31**, 1184 (1985).

[16] S. Saha, R. Palit, J. Sethi, S. Biswas, P. Singh, T. Trivedi, D. Choudhury, and P. C. Srivastava, Phys. Rev. C **89**, 044315 (2014).

[17] S. Saha, R. Palit, J. Sethi, T. Trivedi, P. C. Srivastava, S. Kumar, B. S. Naidu, R. Donthi, S. Jadhav, D. C. Biswas, U. Garg, A. Goswami, H. C. Jain, P. K. Joshi, G. Mukherjee, Z. Naik, S. Nag, V. Nanal, R. G. Pillay, S. Saha *et al.*, Phys. Rev. C **86**, 034315 (2012).

[18] Z. G. Wang, M. L. Liu, Y. H. Zhang, X. H. Zhou, S. Guo, J. G. Wang, X. G. Lei, Y. Zheng, Y. D. Fang, Y. H. Qiang, N. T. Zhang, B. Ding, G. S. Li, F. Ma, X. L. Yan, S. C. Wang, B. S. Gao, F. Fang, B. T. Hu, X. G. Wu *et al.*, Phys. Rev. C **89**, 044308 (2014).

[19] Purnima Singh, R. Palit, S. Saha, J. Sethi, S. Biswas, D. Choudhury, P. C. Srivastava, and T. Trivedi, Phys. Rev. C **90**, 014306 (2014).

[20] X. Z. Cui, L. H. Zhu, X. G. Wu, Z. M. Wang, C. Y. He, Y. Liu, G. S. Li, S. X. Wen, Z. L. Zhang, R. Meng, R. G. Ma, P. Luo, Y. Zheng, M. M. Ndontchueng, J. D. Huo, and C. X. Yang, Phys. Rev. C **72**, 044322 (2005).

[21] P. W. Luo, X. G. Wu, H. B. Sun, G. S. Li, C. Y. He, Y. Zheng, C. B. Li, S. P. Hu, Y. H. Wu, H. W. Li, J. J. Liu, J. L. Wang, S. H. Yao, and Scott A. Edwards, Phys. Rev. C **89**, 034318 (2014).

[22] S. Ray, N. S. Pattabiraman, R. Goswami, S. S. Ghugre, A. K. Sinha, and U. Garg, Phys. Rev. C **69**, 054314 (2004).

[23] N. S. Pattabiraman, S. N. Chintalapudi, S. S. Ghugre, B. V. Tirumala Rao, M. L. N. Raju, T. S. Reddy, P. K. Joshi, R. Palit, and H. C. Jain, Phys. Rev. C **65**, 044324 (2002).

[24] T. Fukuchi, Y. Gono, A. Odahara, S. Tanaka, M. Inoue, Y. Wakabayashi, T. Sasaki, M. Kibe, N. Hokoiwa, T. Shinozuka, M. Fujita, A. Yamazaki, T. Sonoda, C. S. Lee, Y. K. Kwon, J. Y. Moon, and J. H. Lee, Eur. Phys. J. A **24**, 249 (2005).

[25] B. Kharraja, S. S. Ghugre, U. Garg, R. V. F. Janssens, M. P. Carpenter, B. Crowell, T. L. Khoo, T. Lauritsen, D. Nisius, W. Reviol, W. F. Mueller, L. L. Riedinger, and R. Kaczarowski, Phys. Rev. C **57**, 2903 (1998).

[26] D. Rudolph, C. J. Gross, A. Harder, M. K. Kabadiyski, K. P. Lieb, M. Weiszflog, J. Altmann, A. Dewald, J. Eberth, T. Mylaeus, H. Grawe, J. Heese, and K.-H. Maier, Phys. Rev. C **49**, 66 (1994).

[27] M. Hausmann, A. Jungclaus, E. Galindo, K. P. Lieb, O. Yordanov, I. P. Johnstone, R. Schwengner, A. Dewald, A. Fitzler, O. Möller, G. de Angelis, A. Gadea, T. Martinez, D. R. Napoli, and C. Ur, Phys. Rev. C **68**, 024309 (2003).

[28] S. S. Ghugre, B. Kharraja, U. Garg, R. V. F. Janssens, M. P. Carpenter, B. Crowell, T. L. Khoo, T. Lauritsen, D. Nisius, W. Reviol, W. F. Mueller, L. L. Riedinger, and R. Kaczarowski, Phys. Rev. C **61**, 024302 (1999).

[29] F. Ghazi Moradi, C. Qi, B. Cederwall, A. Ataç, T. Bäck, R. Liotta, M. Doncel, A. Johnson, G. de France, E. Clément, A. Dijon, R. Wadsworth, T. W. Henry, A. J. Nichols, H. Al-Azri, J. Nyberg, A. Gengelbach, T. Hüyük, B. M. Nyakó, J. Timár *et al.*, Phys. Rev. C **89**, 014301 (2014).

[30] E. Galindo, M. Hausmann, A. Jungclaus, K. P. Lieb, O. Yordanov, I. P. Johnstone, R. Schwengner, A. Dewald, A. Fitzler, O. Möller, G. de Angelis, A. Gadea, T. Martinez, D. R. Napoli, and C. A. Ur, Phys. Rev. C **69**, 024304 (2004).

[31] A. Jungclaus, D. Kast, K. P. Lieb, C. Teich, M. Weiszflog, T. Härtlein, C. Ender, F. Köck, D. Schwalm, J. Reif, R. Peusquens, A. Dewald, J. Eberth, H.-G. Thomas, M. Górska, and H. Grawe, Nucl. Phys. A **637**, 346 (1998).

[32] R. Schwengner, G. Winter, J. Reif, H. Prade, L. Käubler, R. Wirowski, N. Nicolay, S. Albers, S. Eßer, P. von Brentano, and W. Andrejtscheff, Nucl. Phys. A **584**, 159 (1995).

[33] P. Banerjee, S. Ganguly, M. K. Pradhan, Md. Moin Shaikh, H. P. Sharma, S. Chakraborty, R. Palit, R. G. Pillay, V.

Nanal, S. Saha, and J. Sethi, Phys. Rev. C **98**, 034320 (2018).

[34] S. Saha, R. Palit, J. Sethi, S. Biswas, P. Singh, S. Nag, A. K. Singh, I. Ragnarsson, F. S. Babra, U. Garg, A. Goswami, E. Ideguchi, H. C. Jain, S. Kumar, Md. S. R. Laskar, G. Mukherjee, Z. Naik, and C. S. Palshetkar, Phys. Rev. C **99**, 054301 (2019).

[35] H. Wang, K. Ma, S. Liu, and J. Lu, Chin. Phys. C **45**, 094106 (2021).

[36] R. Palit, in *Application of Accelerators in Research and Industry: Twenty-First International Conference*, edited by F. D. McDaniel and B. L. Doyle, AIP Conf. Proc. No. 1336 (AIP, New York, 2011), p. 573.

[37] H. Tan *et al.*, in *Nuclear Science Symposium Conference Record 2008* (IEEE, Washington, DC, 2008), p. 3196.

[38] R. Palit, S. Saha, J. Sethi, T. Trivedi, S. Sharma, B. S. Naidu, S. Jadhav, R. Donthi, P. B. Chavan, H. Tan, and W. Hennig, Nucl. Instrum. Methods Phys. Res., Sect. A **680**, 90 (2012).

[39] D. C. Radford, Nucl. Instrum. Methods Phys. Res., Sect. A **361**, 297 (1995).

[40] D. C. Radford, Nucl. Instrum. Methods Phys. Res., Sect. A **361**, 306 (1995).

[41] P. J. Twin, in *The Electromagnetic Interaction in Nuclear Spectroscopy*, edited by W. D. Hamilton (North-Holland, Amsterdam, 1975), p. 701.

[42] A. Krämer-flecken, T. Morek, R. M. Lieder, W. Gast, G. Hebbinghaus, H. M. Jäger, and W. Urban, Nucl. Instrum. Methods Phys. Res., Sect. A **275**, 333 (1989).

[43] K. S. Krane, R. M. Steffen, and R. M. Wheeler, At. Data Nucl. Data Tables **11**, 351 (1973).

[44] GTOL code, see https://www-nds.iaea.org/public/ensdf_pgm/.

[45] S. K. Basu and E. A. McCutchan, Nucl. Data Sheets **165**, 1 (2020).

[46] P. M. Jones, L. Wei, F. A. Beck, P. A. Butler, T. Byrski, G. Duchne, G. de France, F. Hannachi, G. D. Jones, and B. Kharraja, Nucl. Instrum. Methods Phys. Res., Sect. A **362**, 556 (1995).

[47] Ch. Droste, S. G. Rohoziński, K. Starosta, T. Morek, J. Srebrny, and P. Magierski, Nucl. Instrum. Methods Phys. Res., Sect. A **378**, 518 (1996).

[48] J. A. Becker, S. D. Bloom, and E. K. Warburton, Am. Chem. Soc. Symp. Ser. **324**, 78 (1986).

[49] N. Shimizu, T. Mizusaki, Y. Utsuno, and Y. Tsunoda, Comput. Phys. Commun. **244**, 372 (2019).

[50] A. Hosaka, K.-I. Kubo, and H. Toki, Nucl. Phys. A **444**, 76 (1985).

[51] X. Ji and B. H. Wildenthal, Phys. Rev. C **37**, 1256 (1988).

[52] D. H. Gloeckner, Nucl. Phys. A **253**, 301 (1975).

[53] F. J. D. Serduke, R. D. Lawson, and D. H. Gloeckner, Nucl. Phys. A **256**, 45 (1976).

[54] D. Bucurescu, C. Rusu, N. Mărginean, C. A. Ur, G. de Angelis, L. Corradi, D. Bazzacco, S. Beghini, F. Della Vedova, G. Duchene, E. Farnea, T. Faul, E. Fioretto, A. Gadea, W. Gelletly, B. Guiot, M. Ionescu-Bujor, A. Iordăchescu, S. D. Landown, S. M. Lenzi *et al.*, Phys. Rev. C **76**, 064301 (2007).